Understanding Substrate Loss in Microwave Acoustic Resonators

Liuqing Gao, Yansong Yang, and Songbin Gong
Department of Electrical and Computer Engineering
University of Illinois at Urbana-Champaign
Urbana, USA
lgao13, yyang165, songbin@illinois.edu

Abstract—This work studies the influence of substrate loss on the performance of acoustic resonators and characterizes the effective substrate resistivity of LiNbO3 thin-film on a high-resistivity Si (HR-Si) wafer. Coplanar waveguides (CPWs) are utilized to extract the effective substrate resistivity of LiNbO3 film on Si over a frequency range from 1 to 40 GHz with two different film thicknesses: 400 nm and 1.6 μ m. The effective resistivities of released and unreleased CPW structures are experimentally extracted and analyzed to show that a suspended structure on a thinner LiNbO3 film has less substrate loss due to a smaller electric field filling factor in the film. As a result, the removal of Si wafer by a release process brings more substrate loss reduction for a thin film than that on a thick film.

Keywords—Microelectromechanical systems, millimeter-wave devices, piezoelectric device, effective resistivity, coplanar waveguide

I. INTRODUCTION

As 5G expands to deliver high data rates, research efforts nowadays focus on scaling front-end technologies towards the 5G high-band (over 24 GHz) where abundant bandwidth is available. Due to increased loss at high frequency, the high-band counterparts of RF transceivers might have degraded performance. The performance degradation must be kept within a reasonable range. Such requirement applies to front-end filters, where improving the loss and enhancing frequency selectivity can significantly improve 5G transceiver performance.

At 5G high-band, miniature filters supporting MIMO operation in handheld are still under development as the small size requirement is still the main hurdle. Acoustic filters have the highest potential due to their small sizes, pervasiveness at RF, and low manufacturing cost. An overmoded acoustic resonator on LiNbO3 thin-film is one great example of the results that such technology development can potentially deliver. Recently, an acoustic resonator utilizing antisymmetric Lamb wave modes on LiNbO₃ thin-film has been demonstrated at frequencies beyond 10 GHz in a compact footprint of 2×10^{-3} mm² [1], promising an excellent resonator platform to enable miniature filters. The resonator can operate up to 56 GHz by exploiting antisymmetric overmodes. Using these antisymmetric modes in LiNbO₃, several follow-up studies have demonstrated hybrid acoustic filters at 14.7 GHz and 19 GHz with on-chip inductors to widen the fractional bandwidth (FBW) by five times the FBW of the acoustic-only counterpart [2]–[4]. As a result of low inductor Q, the hybrid filter suffers from high passband insertion loss. The low inductor Q is mainly caused by high effective substrate loss at high frequency. Maintaining low loss is the major hurdle

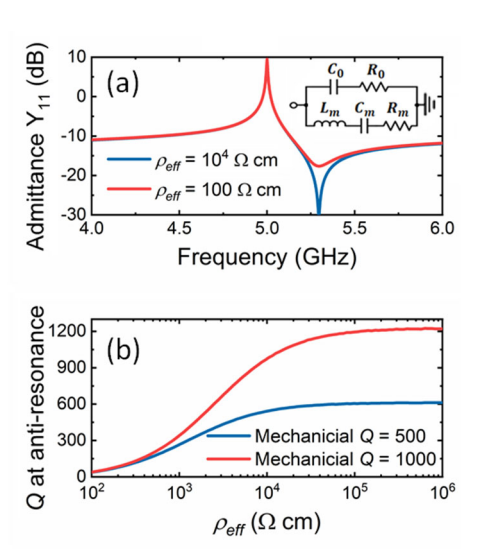


Fig. 1. (a) Admittance of the MBVD circuit model of a resonator with effective substrate resistivity ($\rho_{\it eff}$) of 100 and 10⁴ Ω cm (MBVD circuit model in the inset). (b) The resonator Q at anti-resonance versus $\rho_{\it eff}$ of the substrate with resonator mechanical Q of 500 and 1000.

when scaling RF front-ends to mmWave frequency, as the loss mechanisms that were negligible at low frequency become significant. One of them is the substrate loss of LiNbO₃ thin-film on Si wafer that has not been systematically studied thus far. If substrate loss is not mitigated, it either deteriorates the quality factor of on-chip inductors that can be used to widen the bandwidth of filters, or decreases the anti-resonance Qs of resonators, the main building blocks of acoustic filters. For instance, the Q of an on-chip inductor on suspended LiNbO₃ thin-film is 35 at 7 GHz, which decays fast with increasing frequency to only 8 at 18 GHz [4].

At high frequency, non-ideal substrate loss not only results in deteriorated inductor Qs, but also influences the anti-resonance Qs of acoustic resonators. The admittances of an acoustic resonator with a mechanical Q of 1000 on a substrate with different effective resistivities (ρ_{eff}) of 100 Ω cm and $10^4 \Omega$ cm are plotted in Fig. 1 (a). The non-ideal substrate effective resistivity increases the R_0 in the modified Butterworth–van Dyke (MBVD) model of an acoustic resonator, which influences the anti-resonance Q. The resonator anti-resonance Q versus substrate ρ_{eff} with ρ_{eff} varying from 100 to $10^6 \Omega$ cm is plotted in Fig. 1 (b). With a substrate ρ_{eff} of 100 Ω cm, a resonator with a mechanical Q of 500 would only have a loaded Q of 38, and a resonator with a mechanical Q of 1000 will have a loaded Q of

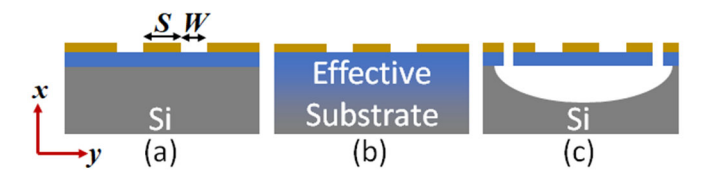


Fig. 2. Cross-section views of a coplanar waveguide on (a) a LiNbO₃ film on Si (test structure), (b) a effective homogeneous substrate, and (c) test structure after release (reference structure).

40. When the substrate ρ_{eff} is low, the loaded Q at anti-resonance is highly dependent on substrate loss.

In either the case of on-chip inductors or acoustic resonators, significant performance cutback has to be made for the filters. To overcome this, one has to understand and characterize the loss mechanisms intrinsic to the device structure. In this work, CPW test structures are fabricated on LiNbO₃ film on an HR-Si wafer with two different film thicknesses to experimentally extract the effective substrate resistivity. Then, the test structures are released to extract the effective substrate resistivity of the suspended structures, which is also called reference structure. Then, the test and reference structures are used to accurately extract the Si wafer resistivity.

II. SUBSTRATE LOSS EXTRACTION USING CPW STRUCTURES

A. Effective Substrate Resistivity

The effective resistivity method proposed by D. Lederer and J.-P. Raskin allows characterization of the substrate loss of planar structures [5]. This method isolates substrate loss from conductor loss, allowing a breakdown understanding of the total RF loss of a CPW. There have been several works using CPW to characterize the substrate loss of SiO₂ film on Si [5] [6], but LiNbO₃ film on Si has not been studied yet. This work utilizes the effective resistivity method to extract the substrate loss of LiNbO₃ film on a Si wafer.

A schematic of the test structure, a CPW structure on LiNbO₃ film on Si, is shown in Fig. 2 (a). The effective substrate is plotted in Fig. 2 (b). The inhomogeneous substrate including the LiNbO₃ film and Si wafer is modelled by a homogeneous effective substrate. The resistivity of the effective substrate (ρ_{eff}) can be expressed by:

$$G_{test} = q \cdot \frac{A}{d \cdot \rho_{eff}} = q \cdot \frac{C_{test}}{\varepsilon_{test}} \cdot \frac{1}{\rho_{eff}}$$

$$\rho_{eff} = q \cdot \frac{C_{test}}{\varepsilon_{test}} \frac{1}{G_{test}}$$
(2)

$$\rho_{eff} = q \cdot \frac{C_{test}}{\varepsilon_{tost}} \frac{1}{G_{tost}} \tag{2}$$

$$q = q_1 + q_2 \tag{3}$$

where q, q_1 , and q_2 are the filling factors of the electric field in the effective substrate, LiNbO₃ film, and Si wafer, respectively. Ctest and Gtest are the capacitance and conductance per unit length in the lumped-element circuit equivalent of the measured CPW test structure. A and d are the area and separation of a parallel plate equivalent of the CPW structure. ε_{test} is the permittivity of the test structure [in Fig. 2 (a)].

Field distribution of the CPW is dependent on the width of the signal line (S) and the gap between the signal line and the

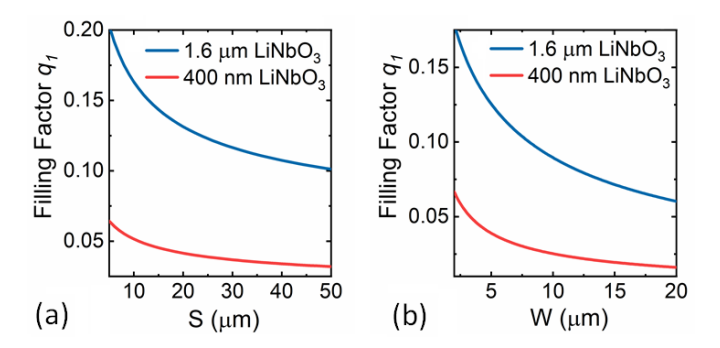


Fig. 3. Filling factor in LiNbO₃ film (q_1) with (a) the width of the signal line (S) of the CPW varying from 5 to 50 µm and (b) the width of the gap between the signal line and ground plane (W) of the CPW varying from 2 to 20 μ m.

ground plane (W). The filling factor of the electric field in the LiNbO₃ film (q_1) can be theoretically predicted by the conformal mapping method [7] [8]. q_1 in LiNbO₃ film with 400 nm and 1.6 μ m thickness with S varying from 5 to 50 μ m and W varying from 2 to 20 µm are plotted in Fig. 3 (a) and (b). The filling factor q_1 is smaller for the thin film LiNbO₃, and decreases with increments in both S and W. With consideration of fabrication limitations on the feature size and the high conductor loss when S is narrow, the gap W is selected to be 4.5 μ m, and S is selected to be 20 μ m.

B. Si Wafer Resistivity

The capacitances per unit length of the test structure (C_{test}) can be expressed by the permittivity and filling factor in the LiNbO₃ film and Si wafer:

$$C_{test} = \varepsilon_{r,test} C_{air} \tag{4}$$

$$\varepsilon_{r\,test} = 1 + q_1(\varepsilon_{r\,LN} - 1) + q_2(\varepsilon_{r\,Si} - 1). \tag{5}$$

where C_{air} is the capacitance per unit length of a CPW surrounded by air [the LiNbO₃ film and Si wafer in Fig. 2 (a) replaced by air]. $\varepsilon_{r,Si}$, $\varepsilon_{r,LN}$ and $\varepsilon_{r,test}$ are the relative permittivity of Si, LiNbO₃, and the test structure [in Fig. 2(a)], respectively. Although LiNbO₃ is an anisotropic material, the $\varepsilon_{r,LN}$ in this work can still be approximated by 45. This is because the CPWs are oriented along the z-axis of X-cut LiNbO₃, such that in the cross-section of the CPW, the x- and y-components of $\varepsilon_{r,LN}$ are both 45. As shown in Fig. 2 (c), the reference structure is the test structure with Si etched away. The reference structure is simulated using the high-frequency structure simulator (HFSS) to confirm that when the release radius is larger than 100 μ m, the ratio of q_2 over q_1 is smaller than 0.2%. The contribution of the Si wafer after release is negligible. As a result, the capacitances per unit length of the reference structure (C_{ref}) has the following expression:

$$C_{ref} = \varepsilon_{r,ref} C_{air} \tag{6}$$

$$\varepsilon_{r,ref} = 1 + q_1 (\varepsilon_{r,LN} - 1) \tag{7}$$

where $\varepsilon_{r,ref}$ is the relative permittivity of the reference structure [in Fig. 2(c)].

The resistivity of the Si wafer (ρ_{Si}) could be extracted by subtracting the capacitance and conductance per unit length of the test structure with reference structure:

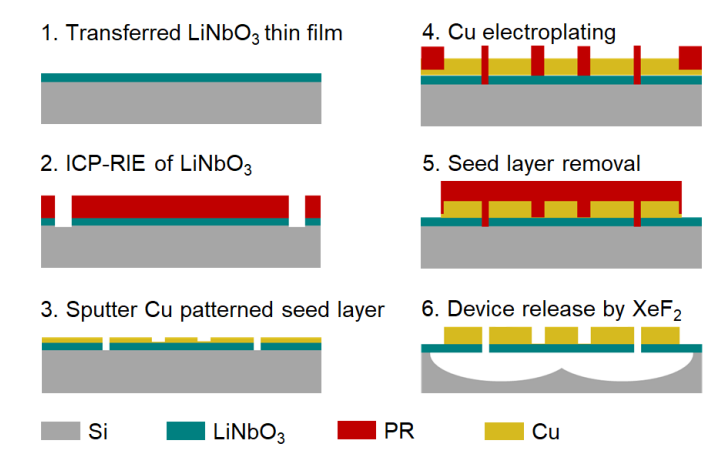


Fig. 4. Fabrication process of the coplanar waveguide (CPW).

$$C_{test} - C_{ref} = q_2 (\varepsilon_{r,Si} - 1) C_{air}$$
 (8)

$$\rho_{Si} = q_2 \cdot \frac{C_{air}}{\varepsilon_0} \frac{1}{G_{Si}} = \frac{C_{test} - C_{ref}}{\varepsilon_0 (\varepsilon_{r,Si} - 1)} \frac{1}{G_{test} - G_{ref}}$$
(9)

This method of subtracting the test structure by reference structure avoids the inaccuracy caused by assuming the filling factor as a constant. Additionally, in this work, the same CPW structure before and after release is used as the test and reference structure, which further reduces any inaccuracy that could cause by the nonuniformity in the thickness of LiNbO₃ film and electroplated Cu layer.

III. FABRICATION AND MEASUREMENT

To study the substrate loss of LiNbO $_3$ on high-resistivity Si, the CPW designs are fabricated, measured, and analyzed on two samples with different X-cut LiNbO $_3$ film thicknesses: 400 nm and 1.6 μ m.

A. Fabrication Process

A brief fabrication process of the CPW structure is shown in Fig. 4. The fabrication starts with an X-cut LiNbO₃ film on a high resistivity silicon wafer. SPR220 is used as the mask for Inductively Coupled Plasma - Reactive Ion Etching (ICP-RIE) of LiNbO₃ film to create release windows. To maintain the small feature size during electroplating, the seed layer is patterned. The metal layer is then thickened by electroplating to reduce the conductor loss. Then, the electroplated region is covered by a layer of photoresist (PR) during seed layer removal using Cu etchant. After step 5, the test structure [in Fig. 2(a)] is obtained and measured. After that, the devices are released by XeF₂ etching of Si to obtain the reference structure [in Fig. 2(c)].

B. Measurement of Test and Reference Structures

Microscope images of the fabricated test structures and suspended reference structures are shown in Fig. 5 and Fig. 6. TRL (Thru, Reflect, Line) calibration is employed to obtain measurement results with a high level of accuracy. As the TRL calibration is most accurate at the electrical length of 90°, CPWs with various lengths ranging from 750 μ m to 3 mm, are fabricated to extract the ρ_{eff} over a frequency range from 1 to 40 GHz. The frequencies at which the various CPW lengths correspond to a quarter wavelength are listed in Table I. The extracted resistivity

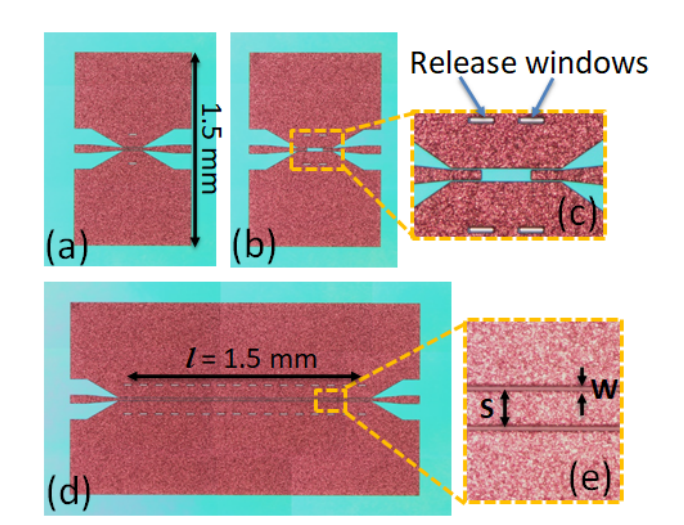


Fig. 5. Microscope image of the fabricated test structure: (a) thru standard, (b) reflection standard, (c) center region of the reflection standard, (d) CPW, and (e) center region of the CPW.

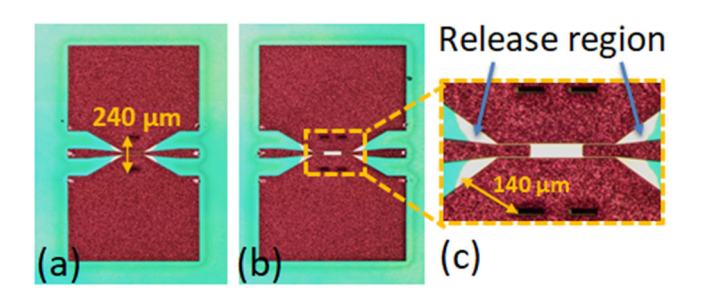


Fig. 6. Microscope images of the fabricated reference structures: (a) thru standard, (b) reflection standard, (c) center region of the reflection standard after release.

TABLE I. FREQUENCY (GHz) WITH CPW LENGTHS CORRESPONDING TO QUARTER WAVELENGTH

	3 mm	2 mm	1.5 mm	1 mm	0.75 mm
400 nm LiNbO ₃	10	15.3	22.6	30	40
1.6 µm LiNbO ₃	9.2	13.8	20.7	27.6	36.8

is obtained by combining the extracted ρ_{eff} in the selected frequency range of the CPW with various lengths.

The extracted $\rho_{\it eff}$ of the released and unreleased LiNbO₃ on Si structures with two different LiNbO₃ thicknesses are plotted in Fig. 7. The improvement in substrate $\rho_{\it eff}$ by Si removal is significant in the low-frequency range. For the 400 nm LiNbO₃ sample, at 5 GHz, the $\rho_{\it eff}$ increases from 185 Ω cm to 840 Ω cm, by 4.5 times, whereas, at 40 GHz the $\rho_{\it eff}$ only increases from 65 Ω cm to 87 Ω cm, by 1.3 times. This indicates that the contribution from Si to the effective substrate loss is more significant in the lower frequency range, whereas LiNbO₃ is the major contributor to the effective substrate loss in the higher frequency range.

The improvement in reducing effective substrate loss due to Si removal is less significant for the thick film structure, namely

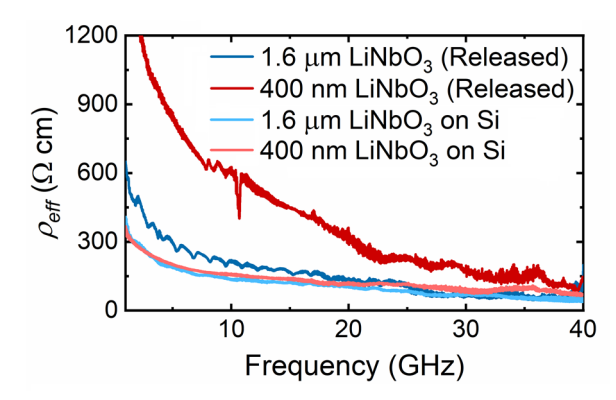


Fig. 7. Extracted effective substrate resistivity ($\rho_{\it eff}$) from the measurement results of CPWs fabricated on 400 nm and 1.6 μ m x-cut LiNbO₃ on Si before and after release.

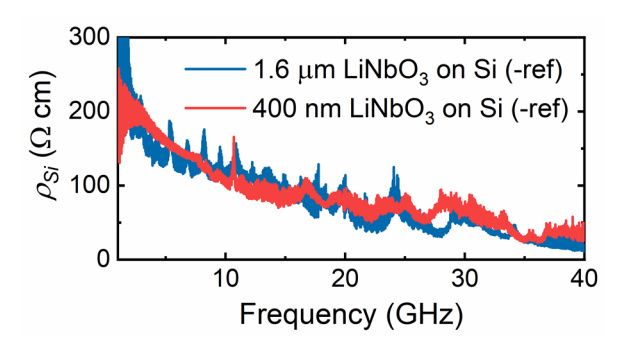


Fig. 8. Extracted Si wafer resistivty (ρ_{Si}) from the measurement results of CPWs fabricated on 400 nm and 1.6 μ m x-cut LiNbO₃ on Si.

1.6 μm LiNbO₃. At 5 GHz, for the 1.6 μm LiNbO₃ sample, the $\rho_{\it eff}$ increases from 190 Ω cm to 295 Ω cm, by only 1.5 times. This is caused by a larger filling factor in the thicker LiNbO₃ film, which results in a larger contribution from the LiNbO₃ film to the effective substrate loss and a smaller contribution from the Si wafer.

The Si wafer resistivities (ρ_{Si} S) extracted from the measurement results of the test and reference structures are plotted in Fig. 8. The loss from the Si wafer is similar in the two

samples with different LiNbO₃ thicknesses. It indicates that the difference in the ρ_{eff} between the two unreleased samples is mainly caused by the different losses from the LiNbO₃ films.

IV. CONCLUSION

In this work, the effective substrate loss of LiNbO₃ on an HR-Si wafer with two different LiNbO₃ film thicknesses has been studied over a frequency range from 1 to 40 GHz. A comparison of released and unreleased structures has also been carried out to conclude that a suspended structure has higher efficiency in reducing the effective substrate loss of thin-film LiNbO₃ on Si than thick film. Additionally, the Si wafer contributes more to the effective substrate loss in the lower frequency range than in the higher frequency range.

ACKNOWLEDGMENT

The authors wish to thank the staff of Nick Holonyak Micro and Nanotechnology Laboratory and the Micro-Nano Mechanical System Cleanroom at University of Illinois at Urbana-Champaign, where the devices were fabricated.

REFERENCES

- [1] Y. Yang, R. Lu, L. Gao, and S. Gong, "10-60-GHz Electromechanical Resonators Using Thin-Film Lithium Niobate," *IEEE Trans. Microw. Theory Tech.*, vol. 68, no. 12, pp. 5211–5220, 2020.
- [2] L. Gao, Y. Yang, and S. Gong, "A 14.7 GHz lithium niobate acoustic filter with fractional bandwidth of 2.93%," in 2020 IEEE International Ultrasonics Symposium, 2020, pp. 1–4.
- [3] L. Gao, Y. Yang, and S. Gong, "A 19 GHz Lithium Niobate Acoustic Filter with FBW of 2.4%," in 2020 MTT-S International Microwave Symposium (IMS), 2020, pp. 1–4.
- [4] L. Gao, Y. Yang, and S. Gong, "Wideband Hybrid Monolithic Lithium Niobate Acoustic Filter in the K-Band," *IEEE Trans. Ultrason. Ferroelectr. Freq. Control*, vol. 68, no. 4, pp. 1408–1417, 2021.
- [5] D. Lederer and J. P. Raskin, "Effective resistivity of fully-processed SOI substrates," Solid. State. Electron., vol. 49, no. 3, pp. 491–496, 2005.
- [6] C. R. Neve and J. P. Raskin, "RF harmonic distortion of CPW lines on HR-Si and trap-rich HR-Si substrates," *IEEE Trans. Electron Devices*, vol. 59, no. 4, pp. 924–932, 2012.
- [7] E. Carlsson and S. Gevorgian, "Conformal mapping of the field and charge distributions in multilayered substrate CPW's," *IEEE Trans. Microw. Theory Tech.*, vol. 47, no. 8, pp. 1544–1552, 1999.
- [8] G. Ramesh, B. Inder, and M. Bozzi, Microstrip Lines and Slotlines. 2013.